Unfolding, Aggregation, and Seeded Amyloid Formation of Lysine-58-Cleaved β_2-Microglobulin†

Niels H. H. Heegaard,*,‡ Thomas J. D. Jørgensen,§ Noémi Rozlosnik,|| Dorthe B. Corlin,‡ Jesper S. Pedersen,⊥ Anna G. Tempesta,# Peter Roepstorff,§ Rogert Bauer,#,○ and Mogens H. Nissen△

Department of Autoimmunology, Statens Serum Institut, DK-2300 Copenhagen S, Department of Molecular Biology, University of Southern Denmark, DK-5230 Odense M, The Danish Polymer Centre, Risø National Laboratory, DK-4000 Roskilde, Department of Life Sciences, Aalborg University, DK-9000 Aalborg, Department of Mathematics and Physics, Royal Veterinary and Agricultural University, DK-1871 Frederiksberg C, and Institute of Medical Anatomy, University of Copenhagen, DK-2200 Copenhagen N, Denmark

Received November 14, 2004; Revised Manuscript Received December 30, 2004

ABSTRACT: β_2-Microglobulin (β_2m) is the amyloidogenic protein in dialysis-related amyloidosis, but the mechanisms underlying β_2m fibrillogenesis in vivo are largely unknown. We study a structural variant of β_2m that has been linked to cancer and inflammation and may be present in the circulation of dialysis patients. This β_2m variant, ΔK58-β_2m, is a disulfide-linked two-chain molecule consisting of amino acid residues 1−57 and 59−99 of intact β_2m, and we here demonstrate and characterize its decreased conformational stability as compared to wild-type (wt) β_2m. Using amide hydrogen/deuterium exchange monitored by mass spectrometry, we show that ΔK58-β_2m has increased unfolding rates compared to wt-β_2m and that unfolding is highly temperature dependent. The unfolding rate is 1 order of magnitude faster in ΔK58-β_2m than in wt-β_2m, and at 37 °C the half-time for unfolding is more than 170-fold faster than at 15 °C. Conformational changes are also reflected by a very prominent Congo red binding of ΔK58-β_2m at 37 °C, by the evolution of thioflavin T fluorescence, and by changes in intrinsic fluorescence. After a few days at 37 °C, in contrast to wt-β_2m, ΔK58-β_2m forms well-defined high molecular weight aggregates that are detected by size-exclusion chromatography. Atomic force microscopy after seeding with amyloid-β_2m fibrils under conditions that induce minimal fibrillation in wt-β_2m shows extensive amyloid fibrillation in ΔK58-β_2m samples. The results highlight the instability and amyloidogenicity under near physiological conditions of a slightly modified β_2m variant generated by limited proteolysis and illustrate stages of amyloid formation from early conformational variants to overt fibrillation.

Deposition of the small (M_r ~12000) seven-stranded β-sandwich protein β_2-microglobulin (β_2m)[1] in joints and connective tissue complicates severe renal failure and long-term hemodialysis treatment (*1*). All hemodialysis patients have significantly elevated serum levels of β_2m (*2*, *3*). β_2m deposits occur in 33% of the cases after four years of dialysis (*4*). The deposits consist of filamentous structures that display the characteristics of amyloid; e.g., insolubility, birefringent staining with Congo red, and unbranched fibrils by electron microscopy (*5*−*7*). The mechanisms by which normal soluble wild-type (wt) β_2m is converted into β_2m-amyloid in vivo are largely unknown but may, as has been suggested for other amyloidogenic β-sheet proteins (*8*), involve partial unfolding or structural rearrangements in parts of the molecule (*9*) leading to the exposure of aggregation-enhancing β-sheet edges (*10*) and stabilization by long-range interactions (*11*). Unmodified wt-β_2m solutions at neutral pH do not form amyloid in vitro even at high concentrations (*12*, *13*), but β_2m-amyloid can be generated from wt-β_2m under acidic conditions (*12*, *14*−*16*) and at neutral pH by seeding wt-β_2m with preformed β_2m-amyloid (*17*) especially in the presence of low concentrations of sodium dodecyl sulfate (*18*). Also, treatment with Cu^{2+} ions (*19*) or exposure to low ionic strength at high protein concentrations (*20*) may lead to fibrillation. Finally, various structurally modified β_2m variants are conformationally unstable and more or less amyloidogenic in vitro (*15*, *21*). While most of the β_2m extracted from ex vivo amyloid deposits is intact, full-length wt-β_2m (*2*, *22*−*24*), about one-third of the material represents processed β_2m, notably species of β_2m lacking the 6 or 19 N-terminal residues, molecules cleaved after other lysine

† Apotekerfonden, The Lundbeck Foundation, M. L. Jørgensen og Gunnar Hansens Fond, The Danish Medical Research Council, and "danmark" Health Care Insurance Foundation have provided economical support. The mass spectrometric investigations were supported by the Carlsberg Foundation and a grant from the Danish Biotechnology Instrument Center funded by the Danish Research Council.

* To whom correspondence should be addressed. Phone: +45 32683378. Fax: +45 32683876. E-mail: nhe@ssi.dk.

‡ Statens Serum Institut.

§ University of Southern Denmark.

|| Risø National Laboratory.

⊥ Aalborg University.

Royal Veterinary and Agricultural University.

○ Deceased.

△ University of Copenhagen.

[1] Abbreviations: AFM, atomic force microscopy; AHS, *N*-(6-aminohexyl)aminopropyltrimethoxysilane; β_2m, β_2-microglobulin; ΔK58-β_2m, cleaved β_2-microglobulin, residues 1−57 and 59−99 of intact β_2m held together by a disulfide bridge; CE, capillary electrophoresis; CR, Congo red; MS, mass spectrometry; SEC, size-exclusion chromatography; ThT, thioflavin T; wt, wild type.

10.1021/bi047594t CCC: $30.25
Published on Web 02/25/2005

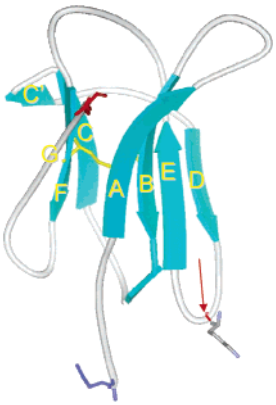

FIGURE 1: Ribbon diagram of the crystal structure of human wt-β_2m (Protein Data Bank number 1LDS) (*9*) drawn using the program WebLab ViewerPro. The disulfide bond connecting Cys-25 (B-strand) and Cys-80 (F-strand) is shown in yellow. Also indicated are the N-terminal side chain (blue), the C-terminal side chain (red), and the Lys-58 side chain (gray). The arrow marks the cleavage site at K58. Individual β-strands are labeled A through G.

residues, and C-terminally truncated forms (*25*−*27*). Some of these variants make amyloid in vitro (*21*) but have not been found in the circulation (*28*). Thus, the question remains if these modified forms along with other posttranslationally modified β_2m molecules (*29*, *30*) are generated before or after amyloid deposition.

With respect to the intact molecules it has recently been shown that a small fraction of wt-β_2m may populate an alternative conformation under physiological conditions and that this heterogeneity is significantly enhanced at low ionic strength and in the presence of organic solvents where the molecule begins to precipitate (*17*, *31*, *32*). Thus, in addition to subtle conformational differences between MHC-complexed and free β_2m (*9*), the molecule in solution is able to populate at least two well-defined conformations, one of which is normally insignificantly populated but more prone to aggregation than the other (*9*, *33*).

Previously, we demonstrated (*34*) that the putative conformational heterogeneity observed in wt-β_2m is much more pronounced in a structural variant of β_2m that can be found in vivo (*35*, *36*). This variant is generated by the concerted action of activated complement and carboxypeptidase B activities in serum (*37*) and consists of a cleaved β_2m molecule lacking lysine-58 (ΔK58-β_2m) (cf. Figure 1). We suggested, primarily on the basis of the increased affinity of one of the two conformers for Congo red and heparin, that ΔK58-β_2m under physiological conditions partially attains a conformation that has amyloidogenic features (*34*).

While wt-β_2m requires acidic pH to significantly exhibit partially unfolded states (*16*) ΔK58-β_2m may do so under neutral pH conditions. However, a conformational heterogeneity of ΔK58-β_2m was previously only indirectly inferred by virtue of its heterogeneous electrophoretic separation patterns (*34*). We here provide direct evidence for increased unfolding, aggregation, and amyloidogenicity of ΔK58-β_2m in comparison with intact wt-β_2m. By using amide hydrogen (^{1}H)/deuterium (^{2}H) exchange monitored by mass spectrometry in addition to capillary electrophoresis, thioflavin T fluorescence spectroscopy, intrinsic tryptophan fluorescence, analytical size-exclusion chromatography with mass-sensitive detection, and atomic force microscopy, we show that ΔK58-β_2m has a pronounced tendency to partially unfold and aggregate especially at physiological temperatures and that it much more readily than wt-β_2m extends amyloid-β_2m fibrils at neutral pH.

EXPERIMENTAL PROCEDURES

Proteins. wt-β_2m and ΔK58-β_2m were purified from nephropathy patient urine as described (*34*−*37*). The preparations of wt-β_2m and ΔK58-β_2m were pure by capillary electrophoresis, reversed-phase HPLC, and mass spectrometry except for 10−20% M99-oxidized species (*32*). By mass spectrometry the molecular masses of the purified proteins were in agreement with the theoretical masses of 11729.2 Da (wt-β_2m) and 11619.0 Da (ΔK58-β_2m). The purified proteins (1−20 mg/mL) in phosphate-buffered saline (PBS) (137 mM NaCl, 2.7 mM KCl, 1.5 mM KH_2PO_4, and 6.5 mM Na_2HPO_4, pH 7.4) were kept at −20 °C until used. Deuterium oxide (D_2O, 99.9 atom % D) was from Cambridge Isotope Laboratories. Deuterated PBS was prepared by lyophilization of protiated buffer followed by redissolution in D_2O. To achieve full deuteration, the deuterated buffers were twice lyophilized and redissolved in D_2O.

Mass Spectrometry and Rapid Desalting. The masses of purified wt-β_2m and ΔK58-β_2m were verified by electrospray ionization (ESI) time-of-flight mass spectrometry using a Mariner biospectrometry workstation (Applied Biosystems, Framingham, MA). Samples from hydrogen/deuterium exchange experiments were analyzed by ESI-MS in positive ion mode on a quadrupole time-of-flight mass spectrometer (Model Micro from Micromass, Manchester, U.K.) coupled to a rapid desalting equipment. The mass spectrometer was calibrated using apomyoglobin. The ion source parameters were capillary voltage 3.1 kV, cone voltage 45 V, ion source block temperature 80 °C, nebulizer gas flow 20 L/h (25 °C), desolvation gas flow 400 L/h (200 °C), and cone gas flow 100 L/h. Nitrogen was used as nebulizer and desolvation gas. The equipment for rapid desalting consisted of two HPLC pumps (one for desalting and one for elution) (Applied Biosystems, Model 140B), a Rheodyne injection valve (Model 7725i), and a timer-controlled Valco 10-port two-position HPLC valve (Model C2-1000A, air actuated) equipped with a self-packed C_{18} microcolumn. Quenched samples from hydrogen/deuterium exchange experiments were thawed individually before injection. The sample was flushed from the injection loop and desalted on the microcolumn for 1 min with a flow of H_2O containing 0.05% (v/v) trifluoroacetic acid (pH 2.2) at 400 μL/min. After desalting, a timer automatically switched the Valco valve and the sample eluted directly into the electrospray ion source with a flow of 70% acetonitrile containing 0.05% (v/v) trifluoroacetic acid at 20 μL/min. The desalted proteins eluted within 1 min. The total time for desalting and elution was 2 min. The solvent precooling coils, Rheodyne injector with loop, and the Valco 10-port valve with microcolumn were immersed in an ice/water slurry (0 °C) to minimize back-exchange with the protiated solvents. The desalting step mainly removes deuterium exchanged for labile hydrogens, i.e., hydrogen attached to N, O, and S in the side chains, and not main chain amide hydrogens at acidic pH (*38*). Thus, the mass increase observed after deuteration and desalting primarily reflects deuterium incorporated into the main chain amide groups.

Hydrogen/Deuterium Exchange Experiments. Hydrogen/deuterium exchange was initiated by dilution (1:50) of the protiated protein solution into deuterated buffer. Typically, 10 μL of an equimolar solution of wt-β_2m and ΔK58-β_2m ($\sim$1 mg/mL in protiated PBS) was added to 490 μL of deuterated PBS, pH 7.3 (value uncorrected for isotope effects). Solutions were maintained at the specified temperatures in a thermomixer. At appropriate intervals, 50 μL aliquots of the exchange solution were withdrawn, and the exchange reaction in the harvested aliquot was quenched by adding 2 μL of 2.5% trifluoroacetic acid (TFA), decreasing the pH to 2.2 (uncorrected value). The samples were stored in liquid N_2 until MS analysis. Back-exchange control experiments were carried out to determine the inevitable deuterium loss that occurs during desalting at quench conditions (pH 2.2 and 0 °C) where the exchange kinetics of main chain amide hydrogens is very slow. Aliquots of fully deuterated wt-β_2m and ΔK58-β_2m at quench conditions (pH 2.2 and 0 °C) were subjected to rapid desalting. Both proteins were observed to have a maximum content of 83 $\pm$ 2 deuterons; i.e., $\sim$10 deuterons are back-exchanged with protons during quench conditions. Note: wt-β_2m contains a total of 93 and ΔK58-β_2m a total of 91 exchangeable main chain amide hydrogens.

MS Data Analysis. The number of incorporated deuterons was determined from the difference between the average mass of the deuterated population and the average mass of the fully protiated protein. The average masses were determined from ESI mass spectra deconvoluted with the Micromass maximum entropy algorithm (MassLynx 3.5 software). No adjustments for deuterium loss or gain during quench conditions were performed since our main focus is the correlated exchange kinetics which is unaffected by such adjustments. To obtain rate constants for the correlated exchange (i.e., the cooperative unfolding) of wt-β_2m and ΔK58-β_2m, the abundances (areas) of the deuterated populations were determined from deconvoluted ESI mass spectra. Subsequently, abundance ratios of the deuterated populations $[I_{low}/(I_{low} + I_{high})]$ were plotted as a function of exchange time, and the unfolding rate constants for the nonoxidized protein and oxidized protein (k_u and $k_{u,ox}$, respectively) were obtained by fitting a biexponential equation (eq 1) to the data.

$$\frac{I_{low}}{I_{low} + I_{high}} = \frac{I_0 e^{-k_u t}}{I_0 + I_{0,ox} e^{-k_{u,ox} t}} \quad (1)$$

where I_{low} is the abundance (area) of the lower mass peak which represents the population of protein molecules that have not yet undergone correlated exchange. I_{high} is the abundance (area) of the higher mass peak which is comprised of two populations with similar masses: one consisting of protein molecules that have exchanged in a correlated manner and one consisting of M99-oxidized protein molecules that have not yet undergone correlated exchange. The fraction of nonoxidized protein (I_0) and oxidized protein ($I_{0,ox}$) in the sample was determined from mass spectra acquired before deuteration. The fraction of oxidized protein remained constant throughout the exchange experiment. The coefficient of variation in determination of k_u in repeated measurements was less than 15%. To ensure the validity of using maximum entropy analysis on the data, the abundance ratios of the deuterated populations $[I_{low}/(I_{low} + I_{high})]$ were also determined by an independent fitting procedure using Gaussian distributions. The results were in excellent agreement (deviation less than 3%) with the abundance ratios obtained from maximum entropy deconvolution.

Capillary Electrophoresis (CE). A Beckman P/ACE 2050 instrument equipped with liquid sample cooling and UV detection was used. Electrophoresis buffer was 0.1 M phosphate (0.081 M Na_2HPO_4 + 0.019 M NaH_2PO_4), pH 7.4. Detection took place at 200 nm, and the separation tube was a 50 μm inner diameter uncoated fused silica capillary (Polymicro Technologies or Beckman Coulter) of 47 cm total length with 40 cm to the detector window. Samples (10−20 μL) were protected against evaporation by overlayed light mineral oil (Sigma) (*32*). A synthetic peptide of the sequence Ac-Pro-Ser-Lys-Asp-OH was used as an internal marker. Separations were typically carried out at 80−100 μA constant current corresponding to field strengths of 200−400 V/cm (*34*). In dye affinity CE experiments using Congo red (CR) as a buffer additive (*32*), a stock solution of CR was prepared by suspending 0.2 mg/mL in electrophoresis buffer and passing the solution through 0.22 μm pore size filters. The precise concentration of CR in the filtrate was subsequently determined by measuring the 488 nm absorbance using the millimolar extinction coefficient of CR of 41.4 (*39*).

Thioflavin T Binding and Tryptophan Fluorescence. Identical concentrations (2.2 mg/mL, 188 μM) of 66 μL of purified β_2m and ΔK58-β_2m were incubated in triplicate at 37 °C in the presence of 20 μM thioflavin T in 384-well black polystyrene plates (Nunc, Roskilde, Denmark). Emitted fluorescence at 502 nm at an excitation wavelength of 450 nm (slit size 9 nm) was recorded using a SpectraMax Gemini XS fluorescence plate reader (Molecular Devices, Sunnyvale, CA). The plate was read every 30 min with 5 min automixing prior to each reading. Data points represent the means of three individual wells with subtraction of background (signal from well with only 20 μM ThT in PBS). The intrinsic tryptophan fluorescence of the same samples was also measured using an excitation wavelength of 280 nm with emission reading at 355 nm.

Size-Exclusion Chromatography (SEC). Size and mass characterization of monomers, oligomers, and aggregates of wt-β_2m and ΔK58-β_2m were achieved by size-exclusion chromatography (SEC) using refractive index and light scattering detection. An LC-10AD HPLC pump from Shimadzu and a Rheodyne injector were coupled to a Superdex 75 column (7.8 × 300 mm, Pharmacia). Void volume was approximately 7 mL. The column eluent passed through a Static light scattering instrument with a laser operating at 690 nm (Dawn EOS equipped with a K2 flow cell; Wyatt Technology) followed by a refractive index detector (RID-10A; Shimadzu). The elution buffer was 10 mM Na_2HPO_4/NaH_2PO_4, pH 7, containing 0.15 M NaCl. All column runs were performed at ambient temperature. α-Lactalbumin (Sigma) was used to calibrate the light scattering detectors, and bovine serum albumin (Sigma) was used to calibrate the molar mass. The concentration of eluted species was calculated from refractive index values using an incremental index of refraction of 1.85×10^{-4} g/L. For molecules of less than 100 kg/mol, the light scattering is considered isotropic, and the weight average molecular mass was

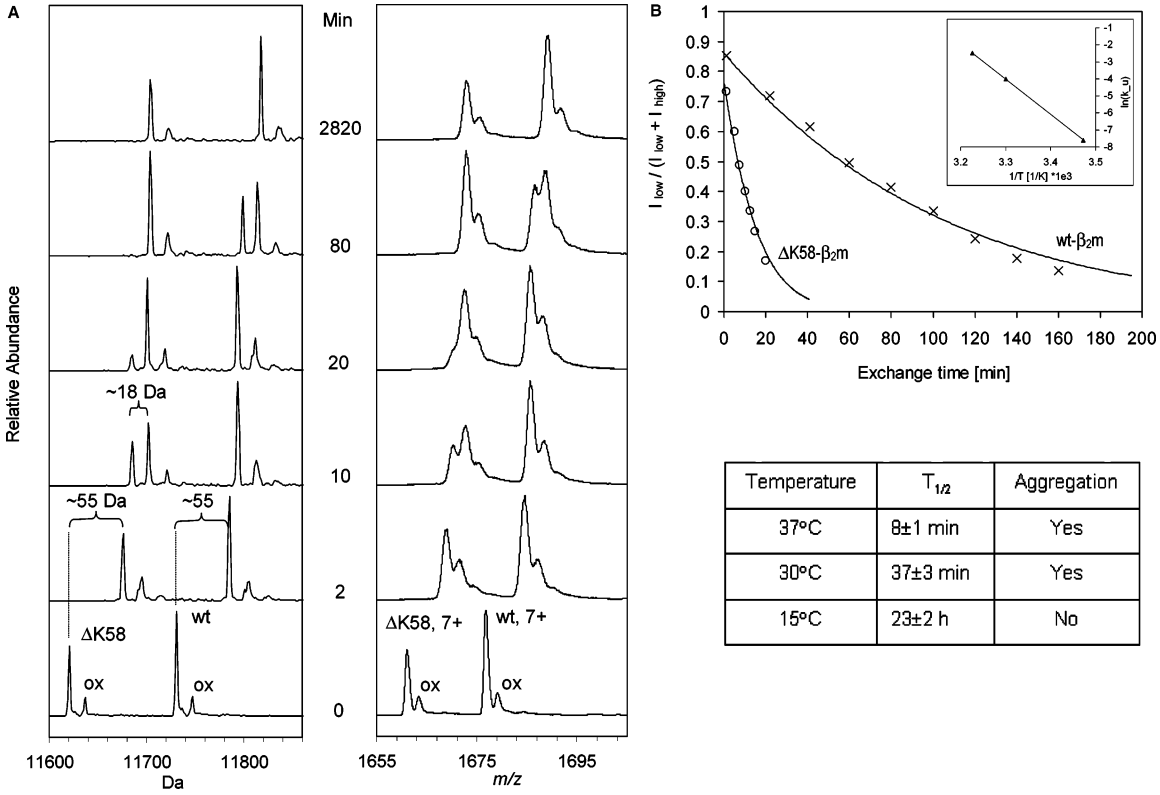

Temperature	$T_{1/2}$	Aggregation
37°C	8±1 min	Yes
30°C	37±3 min	Yes
15°C	23±2 h	No

FIGURE 2: Conformations at 37 °C of wt-β_2m and ΔK58-β_2m characterized by amide hydrogen/deuterium exchange monitored by mass spectrometry. (A) Electrospray ionization (ESI) mass spectra of a mixture of wt-β_2m (wt) and ΔK58-β_2m (ΔK58) obtained after various deuteration periods (given in minutes in the figure) at 37 °C. Left panel: Deconvoluted ESI mass spectra. Right panel: ESI mass spectra of the *m*/*z* region with the $[M + 7H]^{7+}$ ions. The spectra in the left panel represent the deconvoluted (mass transformed) data from the +7 charge state. The spectra obtained at $t = 0$ min (i.e., lowest traces) are obtained from ^1H_2O. Ox = Met-99-oxidized species. (B) Determination of rate constants for the cooperative unfolding of ΔK58-β_2m and wt-β_2m from experiments such as those shown in (A). Ratios of peak areas $[I_{low}/(I_{high} + I_{low})]$ for ΔK58-β_2m (○) and wt-β_2m (×) were plotted as a function of exchange time. The lines show the fits to the experimental data using eq 1 and the constraint $k_u = k_{u,ox}$. The fits were used to estimate the unfolding rate constant, k_u. The insert is an Arrhenius plot of $\ln(k_u)$ as a function of $1/T$ from which the activation enthalpy (E_a) for unfolding was calculated to be 1.7×10^2 kJ/mol. The table summarizes the half-lives for the cooperative unfolding of ΔK58-β_2m and aggregation propensity at different temperatures based on MS-monitored amide hydrogen/deuterium exchange (half-lives), SEC, and CE (aggregation).

obtained as the ratio between the 90 deg detector signal and the refractive index signal calibrated to the ratio obtained for the monomer peak from bovine serum albumin with a molar mass of 66.8 kg/mol. Molar masses are precise to within 5%. In order to estimate the molar mass and radius of gyration of the aggregates, a Berry plot, i.e., the inverse square root of the light scattering signal vs q^2, was made (the light intensities were measured at 15 angles, out of which 10 were used in a q range of 5−24 μm^{-1}). The radius of gyration was derived from the slope of this line and the molar mass from the intercept with the vertical axis.

Fibril Formation from wt-β_2m in Vitro. A solution of 1 mg/mL wt-β_2m was filtered through a 0.22 μm pore size filter and dialyzed in a molecular weight cutoff 3500 dialysis cassette (Pierce) overnight at 4 °C against 0.1 M citric acid/Na_2HPO_4, pH 2.6. After addition of 15 mM NaN_3 the solution (400 μL) was incubated at 37 °C at 300 rpm for 4 days and then kept at 4 °C.

Atomic Force Microscopy. AHS surfaces were made by solution deposition of *N*-(6-aminohexyl)aminopropyltrimethoxysilane (AHS, $C_{12}H_{30}N_2O_3Si$; Gelest Inc., Morrisville, PA) to cleaned silicon [Si(001)] wafers (Topsil, Denmark). AHS solutions were prepared in ambient conditions just before use. For AHS deposition, 0.1 M AHS and 1.5 M MilliQ water were dissolved in 2-propanol (Fisher Scientific). The deposition process was terminated after 3 h by rinsing surfaces in copious amounts of 2-propanol, followed by successive rinsing in a 1:1 water/ethanol mixture and MilliQ water and drying in a stream of argon gas. The quality of the silane monolayers was verified by atomic force microscopy (AFM). The roughness of the surfaces was less than 0.3 nm. Proteins were adsorbed by incubating surfaces with 5 μL proteins in PBS for 0.5 h at ambient conditions. The surfaces were then washed in water and dried in a stream of nitrogen gas. Tapping mode AFM was performed in air at room temperature using a Nanoscope Dimension 3000 (Santa Barbara, CA) equipped with NHC tips from Nanosensors (Neuchatel, Switzerland) with a typical tip radius of 10 nm. The imaging interaction between the tip and the surface was kept as low as possible. All images were flattened using a second-order polynomial algorithm provided with the instrument.

RESULTS

Unfolding of wt-β_2m and ΔK58-β_2m. To probe the solvent accesssibility of the protein backbones of wt-β_2m and ΔK58-β_2m in detail, a series of amide hydrogen/deuterium exchange experiments monitored by mass spectrometry (MS) were carried out (Figure 2). The wild type and ΔK58 variant differ sufficiently in masses to be readily allowed to deuterium-exchange together in the same solution followed by MS

analysis (Figure 2A). When incubating in deuterated buffer at 37 °C, we observed the evolution of a bimodal mass distribution pattern showing that ~18 of about 29 previously protected amide hydrogens exchanged in a correlated manner; i.e., they exchanged simultaneously (Figure 2A). This suggests the occurrence of unfolding events with lifetimes sufficiently long to allow complete exchange of 18 amide hydrogens within a single opening event. The lower mass peaks represent a population of molecules that has not yet unfolded while the higher mass population at +18 Da represents molecules that have unfolded cooperatively together with oxidized species that have not yet cooperatively unfolded. Unfolding events are observed in both the ΔK58-β_2m and the wt-β_2m samples, but the correlated exchange evolves faster in the ΔK58 variant than in the intact molecule. As seen in Figure 2A the higher mass population of ΔK58-β_2m is more abundant than the lower mass population already after 10 min of deuteration. In the case of wt-β_2m at least 80 min is required to populate the higher mass population to the same degree. Thus, ΔK58-β_2m unfolds almost an order of magnitude faster than wt-β_2m. To ensure that the higher mass population did not represent an irreversibly unfolded conformation, protiated ΔK58-β_2m and wt-β_2m were incubated at 37 °C for 6 h before deuteration was initiated. The correlated exchange kinetics was identical to that observed without long-term preequilibration at 37 °C (data not shown), and thus the observations (Figure 2) are caused by a conformational equilibrium. In additional deuterium exchange-out experiments (data not shown) the mass of the protein was observed to decrease as a function of exchange time. This confirms that the appearance of bimodal peaks is the result of a correlated exchange of amide hydrogens and not, for example, due to an oxidation reaction. The number (18 protons) of amide protons cooperatively exchanged would suggest a regional unfolding. However, the precise number of amide hydrogens that is unprotected upon unfolding could be higher since deuterium incorporated prior to the unfolding event may be part of the structure that unfolds (and that exchange will be mass silent).

Surprisingly, no difference in the number of incorporated deuterons resulting from the uncorrelated slow exchange is observed between ΔK58-β_2m and wt-β_2m; i.e., the mass shift of the low mass population as a function of exchange time is identical. The identical levels of protection of the folded conformations indicate that the overall conformations of ΔK58-β_2m and wt-β_2m are quite similar. Theoretically, it would be possible for two different conformations to exhibit the same level of protection, but apart from small differences the far-UV circular dichroism data for the two species are too similar to support this possibility (*34*). It thus appears that the β_2m cleavage and deletion of K58 do not cause a decrease in the number of protected amide hydrogens. Only the stability of the protein is decreased by the backbone cleavage as also indicated by the enhanced propensity of ΔK58-β_2m compared to wt-β_2m to attain a second conformation in specific buffer environments (*34*). Cleavage of the main chain would be expected to increase the local flexibility of the polypeptide chain and cause acceleration of amide hydrogen exchange in nearby residues (*40*). However, K58 resides in a flexible loop (*9*, *41*) where very fast exchange rates would be expected at all times (*42*). Increased flexibility in such loop structures will not be detected by the present type of experiments where only the slowly exchanging main chain amides are monitored.

The cooperative fluctuation discovered here occurs with an unfolding rate equal to the rate of the correlated mass change because the refolding rate of the part of the molecular structure where exchange takes place is much lower than the intrinsic hydrogen exchange rate (a situation known as the EX1 limit of hydrogen exchange) (*43*, *44*). Thus, unfolding rate constants can be estimated by fitting the abundance of the low and high mass populations at various deuteration periods to eq 1 (see Experimental Procedures) using the constraint $k_u = k_{u,ox}$. Unfolding rate constants of 9×10^{-3} min^{-1} for wt-β_2m and 8×10^{-2} min^{-1} (i.e., 9 times faster) for ΔK58-β_2m are determined in this way at 37 °C (Figure 2B). Calculating without constraints gives slightly better fits and an unfolding rate for oxidized species approximately twice the values for the nonoxidized proteins. This suggests that M99-oxidized β_2m species may have a greater propensity for cooperative unfolding, but further experiments will be needed to confirm this result. The unfolding rate constant of ΔK58-β_2m was subsequently determined at different temperatures. We find that going from 15 to 37 °C increases the rate of unfolding of ΔK58-β_2m more than 150 times. This translates into the half-times of the cooperative unfolding listed in the table in Figure 2B. From this set of data an activation enthalpy of 1.7×10^2 kJ/mol for the unfolding of ΔK58-β_2m is estimated (insert, Figure 2B).

Amyloid Dye Binding. Capillary electrophoresis (CE) separates two peaks (f, fast, and s, slow) in ΔK58-β_2m, and one of these peaks has a higher affinity for the amyloid dye Congo red (CR) than the other (*34*). We have interpreted this observation as due to the existence of two slowly interchanging conformations of ΔK58-β_2m and therefore expected a change in the separation profile with a change in analysis temperature. The experiments shown in Figure 3 confirm these assumptions. Thus, while analysis at 16 °C in the presence of 10 μM CR (Figure 3A) shows a separation pattern corresponding to the one previously reported at 20 °C (*34*), analysis at 37 °C (Figure 3B) indicates the participation of all available ΔK58-β_2m in the complex with CR since no peak corresponding to free ΔK58-β_2m is detected. At 37 °C the unfolding is accelerated, and the protein yields one peak in the CE profile (insert, Figure 3B). In contrast, the degree of interaction of wt-β_2m with 10 μM CR at 37 °C (Figure 3C) is limited. Since binding to Congo red is likely to involve hydrophobic forces (*34*), these results indicate that the temperature-favored conformation is more hydrophobic and thus more unfolded than the native conformation represented by wt-β_2m and by the fast (f), less reactive fraction of ΔK58-β_2m. The experiments provide no information about the spectral characteristics of the bound CR, and thus the results do not indicate that the s-fraction attains an amyloid-like conformation but merely that these species are conformationally different from the species represented by the f-fraction.

The potential of ΔK58-β_2m for amyloid formation was compared with wt-β_2m by incubation at 37 °C with thioflavin T (ThT) followed by fluorescence spectroscopy (Figure 3D). The intrinsic tryptophan fluorescence of the samples was recorded at the same time (Figure 3E). ThT is a dye that changes fluorescence when binding to amyloid (*45*). The

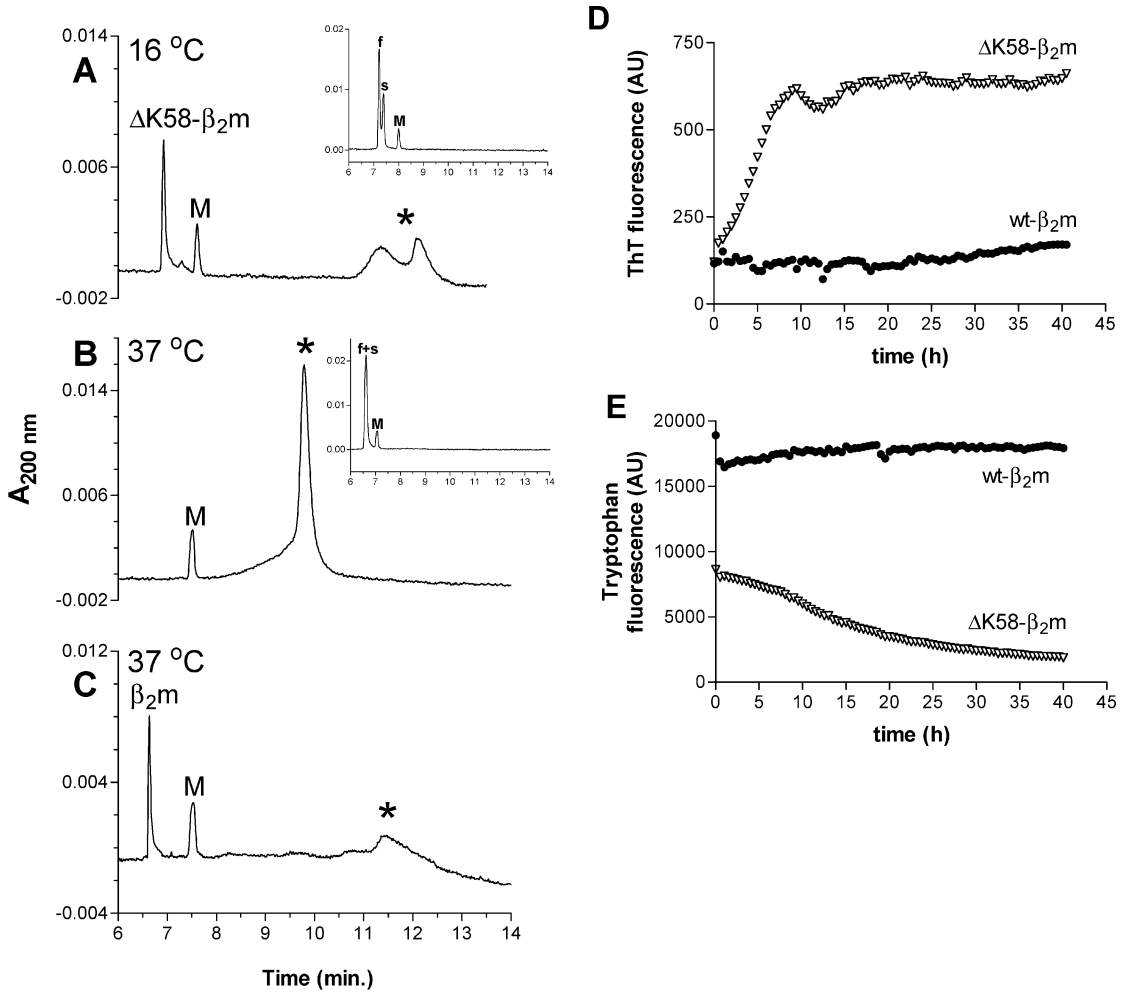

FIGURE 3: Temperature dependency of dye binding to ΔK58-β_2m. (A−C) Capillary electrophoresis (CE) of ΔK58-β_2m and wt-β_2m in the presence of Congo red. The electrophoresis buffer was 0.1 M phosphate, pH 7.38, and samples were pressure-injected for 8 s corresponding to a sample volume of 9 nL and electrophoresed at a constant current of 90 μA. Samples [A, B, ΔK58-β_2m (0.38 mg/mL, 33 μM); C, wt-β_2m (0.21 mg/mL, 18 μM)] were mixed with 0.04 mg/mL marker peptide (82 μM) (M). Affinity CE experiments with 10 μM Congo red added to the electrophoresis buffer were carried out at 16 °C (A) and 37 °C (B, C). Inserts show separations in the absence of CR. Asterisks indicate ΔK58-β_2m and β_2m-CR complex peaks appearing with CR in the running buffer. The panel in (A) is shifted −0.5 min to allow alignment of marker peaks. (D, E) Thioflavin fluorescence and intrinsic tryptophan fluorescence of ΔK58-β_2m (triangles) and wt-β_2m (filled circles) incubated at 37 °C. (D) Fluorescence spectroscopy shows increased thioflavin T staining of ΔK58-β_2m over time. β_2m and ΔK58 (both 2 mg/mL, 170 μM) were incubated at 37 °C in the presence of 20 μM thioflavin T. Emitted fluorescence at 502 nm at an excitation wavelength of 450 nm was recorded every 30 min using 5 min automixing prior to each read. Data points represent the means of three individual wells with subtraction of background (signal from well with only 20 μM ThT in PBS). (E) Tryptophan fluorescence of the same samples measured using an excitation wavelength of 280 nm with emission recording at 355 nm.

results show increased amyloidogenesis in ΔK58-β_2m at 37 °C. The fluorescence signal from ThT in the ΔK58-β_2m sample reaches a maximum after 10 h after a very short lag time. The wt-β_2m signal only slightly increases late in the experiment. The measurements of tryptophan fluorescence in the two samples (Figure 3E) show a decrease in the fluorescence of ΔK58-β_2m over time. This intrinsic fluorescence change indicates that the conformation of ΔK58-β_2m changes over time in the experiment. In contrast, the wild-type protein exhibits no discernible change in tryptophan fluorescence; i.e., the environment of the tryptophan residues is constant (but different from the cleaved β_2m molecule) in this case. A correlation between ThT and Trp fluorescence has been noted in other studies of amyloid formation (*46*). At the onset of the experiment the fluorescence signals are quite different despite identical molar concentration of proteins, and this could be because one or both of the Trp residues of β_2m are more solvent-exposed in ΔK58-β_2m. In accordance with this, one of the residues (Trp-60) is adjacent to the K58 cleavage site. The reason the ThT signal intensity reaches a maximum long before the Trp fluorescence reaches a minimum is possibly because there is a limiting amount of ThT present. Taken together, the experiments in Figure 3 indicate that amyloidogenesis occurs at 37 °C in ΔK58-β_2m but not in wt-β_2m. This is consistent with our finding that preparations of >1 mg/mL purified ΔK58-β_2m, in contrast to wt-β_2m, precipitate out of solution when kept at room temperature for longer periods (data not shown).

Characterization of Aggregation. Since the above experiments indicated a markedly accelerated unfolding rate and increased amyloid-like aggregation of ΔK58-β_2m at physiological temperature, we next used CE and SEC to characterize the temperature influence on aggregation and solubility over time (Figure 4). CE experiments show marked changes in the separation profile of ΔK58-β_2m after incubating for 90 h at 30 °C (Figure 4A). Late peaks appear and most of the starting material disappears. Reversal to lower incubation

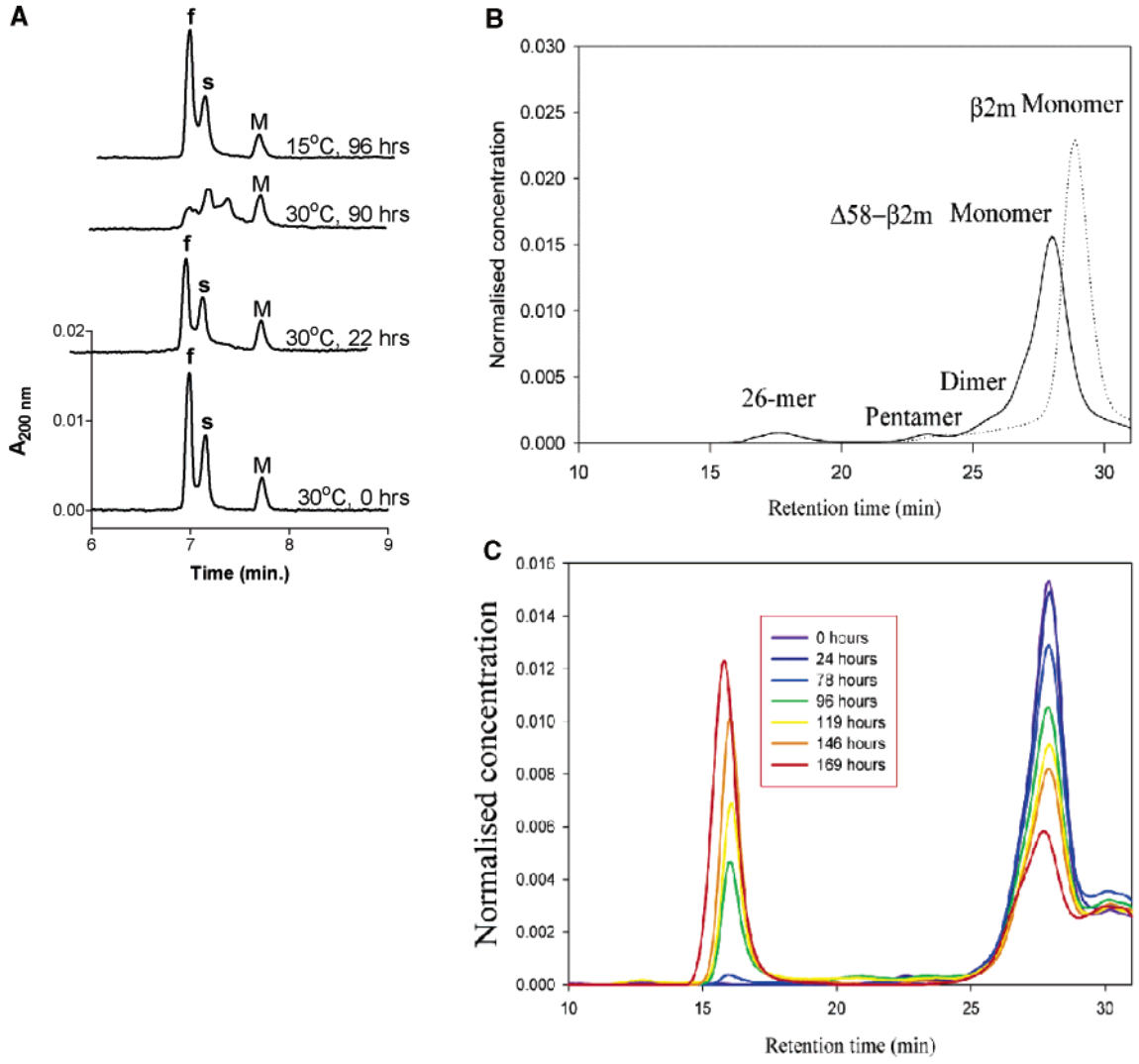

FIGURE 4: Temperature dependency of ΔK58-β_2m aggregation. (A) Time course measurements by capillary electrophoresis of ΔK58-β_2m incubated at 30 °C or at 15 °C. Samples were mixtures of a marker peptide (M) at 0.08 mg/mL (164 μM) and ΔK58-β_2m or wt-β_2m at a final concentration of 0.18 mg/mL (16 μM) in electrophoresis buffer (0.1 M phosphate, pH 7.38). Samples (20 μL) were overlayed by 20 μL of light mineral oil, pressure-injected for 8 s corresponding to a sample volume of 9 nL, and electrophoresed at a constant current of 90 μA. CE was performed using a temperature of 15 °C for the capillary cooling fluid. ΔK58-β_2m is separated into a fast (f) and a slow (s) component (*34*). (B) Size-exclusion chromatography (SEC) analysis of ΔK58-β_2m and wt-β_2m. Overlayed elution profiles of ΔK58-β_2m (solid line) and wt-β_2m (dashed line) as detected by light scattering (signals normalized to the same total amount). Samples (100 μL) of ΔK58-β_2m and wt-β_2m at 1.6 mg/mL were analyzed at a flow rate of 0.5 mL/min. The elution position of monomeric ΔK58-β_2m is approximately 1 min earlier than monomeric wt-β_2m. Also indicated are the positions of peaks corresponding to dimers and higher oligomers in the ΔK58-β_2m sample. (C) ΔK58-β_2m aggregation at 37 °C monitored by SEC. A sample of ΔK58-β_2m at 1.6 mg/mL was kept at 37 °C for several days, and sample aliquots diluted three times in column buffer to a final volume of 100 μL were analyzed at the times points indicated. After a lag phase of about 70 h a considerable increase in an aggregate peak eluting just after 15 min was observed.

temperatures did not normalize the separation profile; i.e., the changes were irreversible. The separation profile of ΔK58-β_2m, however, remained unaffected after incubation at 15 °C for the same time. In CE, the composition of the late peaks appearing upon 30 °C incubation cannot readily be determined since CE is a nonpreparative technique and since migration time in CE is a complicated function of size, shape, and charge (*47*).

In the SEC experiments ΔK58-β_2m elutes approximately 1 min earlier than wt-β_2m despite almost identical detected molecular masses. The larger hydrodynamic volume of monomeric ΔK58-β_2m (Figure 4B) is consistent with conformational heterogeneity. Additional peaks at 17−18 and 23 min and the front tailing asymmetry of the ΔK58-β_2m-peak indicate the presence of small fractions of oligomers in ΔK58-β_2m preparations even at room temperature. The size of these oligomeric species corresponds to 20−30-mers, pentamers, and dimers, as noted in the figure (Figure 4B). No distinct heterogeneity except for front tailing, albeit to a lesser degree than for ΔK58-β_2m, is observed for wt-β_2m under the same experimental conditions (Figure 4B).

While incubation of ΔK58-β_2m for 96 h at 15 °C does not change the SEC profile appreciably from the profile shown in Figure 4B (data not shown), incubation at 37 °C induced pronounced changes. The emergence of large, well-defined aggregates is observed after about 70 h of incubation at 37 °C (Figure 4C). The time scale of the changes observed in the CE experiments (Figure 4A), i.e., late peaks are clearly present after 3−4 days at 30 °C, is in agreement with these observations, but a more detailed characterization of the

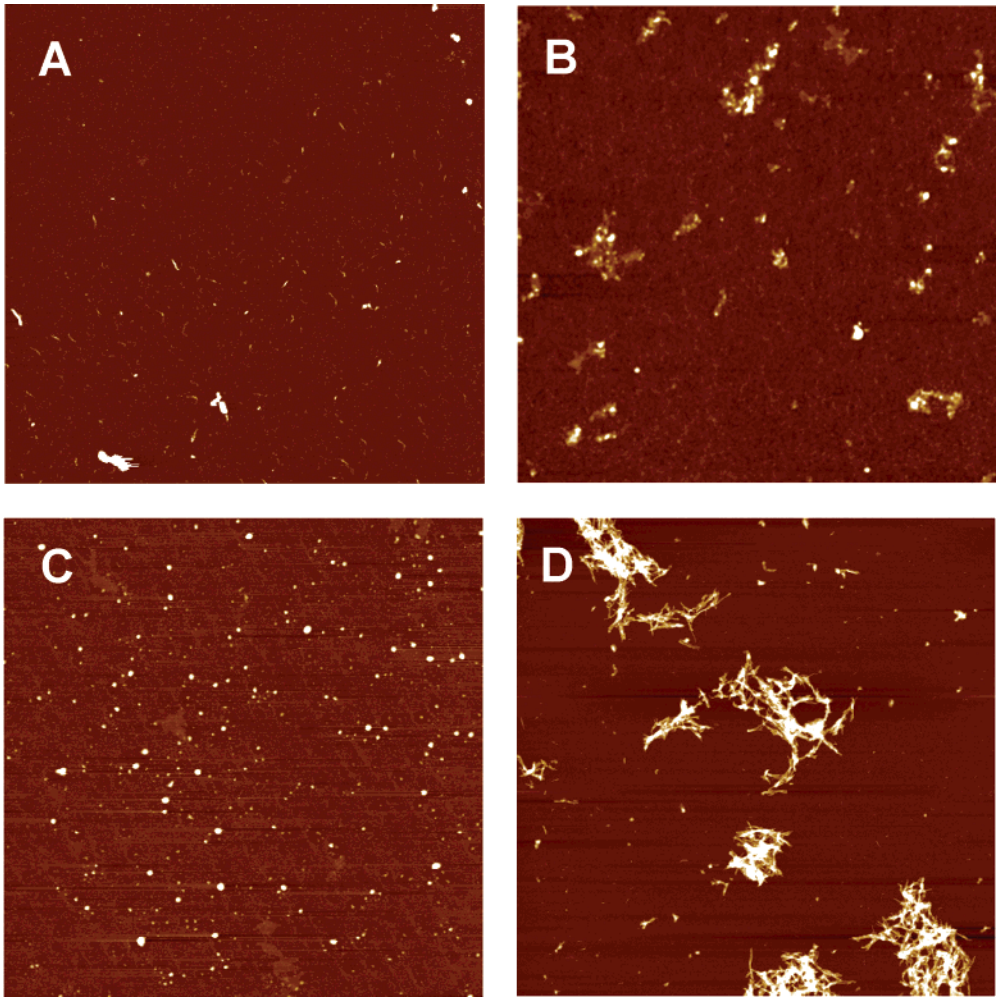

FIGURE 5: Atomic force microscopy (AFM) of β_2m/ΔK58-β_2m preparations adsorbed onto AHS-silicon wafers. Samples (1 mg/mL in PBS) of wt-β_2m and ΔK58-β_2m were incubated for 8 days at 37 °C at 400 rpm. Five microliter aliquots of wt-β_2m (A) and ΔK58-β_2m (C) were applied to AHS-derivatized silicon wafers and examined by tapping mode AFM at a scanning speed of 5 μm/s. The same samples after 30 min incubation with 10% β_2m-amyloid fibrils (preformed from wt-β_2m incubated at pH 2.6 for 4 days at 37 °C) and 30 min drying on the wafers are examined in (B) wt-β_2m and (D) ΔK58-β_2m. The false color scale is 50 nm, and the width of each image is 10 μm (figure reproduced at 75% of original size).

analyte is possible in SEC. Thus, after the lag phase of about 70 h an increasing fraction of large multimers appear just after the column void volume with a corresponding decrease in the area of the monomer peak. The constant elution position of the aggregate peaks indicates that these multimers are of well-defined sizes and masses. The radius of gyration of the aggregate species is 50 nm, and the molecular mass is estimated to be 5×10^6 g/mol corresponding to the presence of about 425 ΔK58-β_2m monomers in the aggregate peak. The relation between mass and radius of gyration of the aggregate peaks is consistent with an internal fibrillar structure of the aggregates. The presence of a lag phase suggested that molecular intermediates interact cooperatively in the aggregation process. No aggregates were observed in wt-β_2m samples when heating at 37 °C for 1 week under the same conditions (data not shown).

ΔK58-β_2m Fibrillogenesis. Atomic force microscopy (AFM) imaging (Figure 5) shows that ΔK58-β_2m has produced numerous spherical assemblies but no discernible fibrillar strutures after incubation for 8 days at 37 °C (Figure 5C) despite the demonstrated specific ThT-binding characteristics of these solutions (Figure 3D). Similar observations were recently reported for a ThT-stainable sample of Aβ-peptide (*48*). ThT binding does not necessarily by itself indicate the presence of amyloid structures (*49*). Visible aggregates are less abundant in the wt-β_2m control (Figure 5A). The effects of seeding with preformed amyloid fibers were next studied (Figure 5B,D). Upon addition of 10% fibrillar seeds there is a very rapid (0.5−1 h) and extensive conversion of aggregates into numerous distinct fibrils and fibril bundles in the ΔK58-β_2m sample (Figure 5D). The fibrils are relatively short; i.e., estimated average lengths are around 400 nm and diameters are less than 25 nm. In this regard these fibrils are reminiscent of the fibrils that can be induced in wt-β_2m solutions under acidic conditions at high ionic strength (*50*). In contrast, in the seeded wt-β_2m sample (Figure 5B) only minor fibrillation is observed in the same time range.

DISCUSSION

A wide range of biophysical and biochemical techniques are needed to study protein folding (*51*). Amyloidogenic proteins have the ability to form partly unfolded species that are prone to aggregate because they expose surfaces favoring intermolecular associations, e.g., edge-to-edge interactions, or because they display extended lengths of polypeptide main

chain engaging in hydrogen bonding (*9*, *10*, *52*, *53*). Thus, an increased population of alternatively folded states probably is an important early event in amyloidogenicity (*54*, *55*). Previously, we reported indirect evidence that ΔK58-β_2m is more conformationally heterogeneous than wt-β_2m (*34*). In the present study we systematically compare ΔK58-β_2m and intact β_2m at 37 °C with respect to unfolding reactions and amyloid dye binding, aggregation, and capacity for extension reactions with amyloid-β_2m. The results show that ΔK58-β_2m cooperatively unfolds in a highly temperature-dependent fashion and, furthermore, that at 37 °C aggregate species with amyloid characteristics appear. Thus, while wt-β_2m is conformationally homogeneous, does not aggregate, and remains in solution at 37 °C, ΔK58-β_2m displays significant rates of cooperative unfolding, stains with the amyloid-specific dyes thioflavin T and Congo red, and, after a lag phase with increasing dye binding but no extensive aggregation, forms large well-defined aggregates. Also, K58-cleaved β_2m extends amyloid fibrils much more readily upon seeding with amyloid-β_2m than does the intact protein.

The ability of ΔK58-β_2m, a species that may be generated in vivo (*56*), to unfold and aggregate under physiological conditions and the striking effect of temperature on the conformational stability of this molecule in contrast to the intact species have not previously been described. The significant temperature dependency was evident in all experiments (cf. table in Figure 2). With half-lives for the unfolding reaction of 8 min at 37 °C and 23 h at 15 °C the probability of intermolecular encounters between two transiently unfolded molecules is dramatically decreased when the temperature is lowered. In accordance with its lack of amyloidogenicity wt-β_2m shows much slower unfolding kinetics with much less chance of an aggregation-prone molecular encounter between unfolded conformers. Hydrogen-exchanged conformers of an amyloidogenic variant of lysozyme were recently charaterized using both NMR and MS, and these results also showed that cooperative unfolding was involved in events predating amyloid formation albeit at higher unfolding rates than we find here (*52*).

The results of the present study thus indicate that unfolded ΔK58-β_2m may behave as a monomeric amyloidogenic intermediate under physiological conditions. The relevance of these observations to β_2m-amyloid formation in patients in vivo remains unclear. ΔK58-β_2m has not been demonstrated in amyloid deposits obtained from patients, and the present experiments have not addressed the amyloid nucleation capabilities of ΔK58-β_2m with wt or other modified forms of β_2m. However, despite reports that β_2m-amyloid only contains unmodified β_2m (*23*, *24*), others have convincingly shown the presence of various modified forms of β_2m in the deposits (*25*, *27*, *57*). The extractability of modified β_2m species thus appears to be an issue. Also, in contrast to other modified forms of β_2m identified in vivo (*15*), ΔK58-β_2m aggregates and is competent to form amyloid fibrils under near physiological conditions in a relatively short period of time. It was recently proposed (*58*) that β_2m residues 59−71 may be important for the self-association of β_2m into amyloid fibrils. It is conceivable that this region [encompassing the β strand E (*9*)] (cf. Figure 1) is less conformationally constrained in ΔK58-β_2m where the backbone is cleaved at K58 just in front of this region and therefore is more likely to be able to participate in intermolecular aggregation. Activation of the complement system by the hemodialysis procedure (*59*) in conjunction with chronically elevated β_2m levels in plasma may generate K58-cleaved β_2m at levels important for amyloidogenesis in joints and connective tissue, but an interplay between wt-β_2m and ΔK58-β_2m in dialysis-related amyloidosis remains speculative especially because ΔK58-β_2m has not yet been found in amyloid tissue extracts (*27*). Also, in the absence of information of the half-lives and fate of cleaved β_2m in the circulation, it is not possible to know if cleaved β_2m will contribute to or actually counteract in vitro amyloidogenesis. The present study highlights the need to investigate whether the population of circulating β_2m as well as carefully extracted amyloid contains cleaved β_2m molecules. Also, it will be relevant to further characterize the folding dynamics of M99-oxidized species and of ΔK58-β_2m in plasma from normal individuals and in plasma from kidney disease patients as well as defining levels, half-lives, and removal mechanisms for ΔK58-β_2m circulating in such patients. Finally, single residue resolution methods such as NMR are very likely to further the structural and mechanistic understanding of the interactions of semidenatured states of ΔK58-β_2m responsible for amyloidogenicity.

ACKNOWLEDGMENT

This paper is dedicated to the memory of Professor Rogert Bauer. Ms. Marianne Lund Jensen is acknowledged for excellent technical assistance with the SEC experiments.

REFERENCES

1. Drüeke, T. B. (2000) β_2-microglobulin and amyloidosis, *Nephrol., Dial., Transplant. 15* (Suppl. 1), 17−24.
2. Gejyo, F., Homma, N., Suzuki, Y., and Arakawa, M. (1996) Serum levels of β_2-microglobulin as a new form of amyloid protein in patients undergoing long-term hemodialysis, *N. Engl. J. Med. 314*, 585−586.
3. Dixit, M. P., Cabansag, M. R., Piscitelli, J., Greifer, I., and Silverstein, D. M. (1999) Serum β_2-microglobulin and immunoglobulin levels in young hemodialysis patients, *Pediatr. Nephrol. 13*, 139−142.
4. Jadoul, M., Garbar, C., Noel, H., Sennesael, J., Vanholder, R., Bernaert, P., Rorive, G., Hanique, G., and van Ypersele, d. S. (1997) Histological prevalence of beta 2-microglobulin amyloidosis in hemodialysis: a prospective post-mortem study, *Kidney Int. 51*, 1928−1932.
5. Nishi, S., Ogino, S., Maruyama, Y., Honma, N., Gejyo, F., Morita, T., and Arakawa, M. (1990) Electron-microscopic and immunohistochemical study of beta-2-microglobulin-related amyloidosis, *Nephron 56*, 357−363.
6. Inoue, S., Kuroiwa, M., Ohashi, K., Hara, M., and Kisilevsky, R. (1997) Ultrastructural organization of hemodialysis-associated β_2-microglobulin amyloid fibrils, *Kidney Int. 52*, 1543−1549.
7. Sunde, M., Serpell, L. C., Bartlam, M., Fraser, P. E., Pepys, M. B., and Blake, C. C. (1997) Common core structure of amyloid fibrils by synchrotron X-ray diffraction, *J. Mol. Biol. 273*, 729−739.
8. Kelly, J. W. (1998) The alternative conformations of amyloidogenic proteins and their multi-step assembly pathways, *Curr. Opin. Struct. Biol. 8*, 101−106.
9. Trinh, C. H., Smith, D. P., Kalverda, A. P., Phillips, S. E., and Radford, S. E. (2002) Crystal structure of monomeric human beta-2-microglobulin reveals clues to its amyloidogenic properties, *Proc. Natl. Acad. Sci. U.S.A. 99*, 9771−9776.
10. Richardson, J. S., and Richardson, D. C. (2002) Natural beta-sheet proteins use negative design to avoid edge-to-edge aggregation, *Proc. Natl. Acad. Sci. U.S.A. 99*, 2754−2759.
11. Krebs, M. R., Morozova-Roche, L. A., Daniel, K., Robinson, C. V., and Dobson, C. M. (2004) Observation of sequence specificity in the seeding of protein amyloid fibrils, *Protein Sci. 13*, 1933−1938.

12. McParland, V. J., Kad, N. M., Kalverda, A. P., Brown, A., Kirwin-Jones, P., Hunter, M. G., Sunde, M., and Radford, S. E. (2000) Partially unfolded states of beta(2)-microglobulin and amyloid formation in vitro, *Biochemistry 39*, 8735−8746.
13. Ono, K., and Uchino, F. (1994) Formation of amyloid-like substance from beta-2-microglobulin in vitro, *Nephron 66*, 404−407.
14. Naiki, H., Hashimoto, N., Suzuki, S., Kimura, H., Nakakuki, K., and Gejyo, F. (1997) *Amyloid Int. J. Exp. Clin. Invest. 4*, 223−232.
15. Kad, N. M., Thomson, N. H., Smith, D. P., Smith, D. A., and Radford, S. E. (2001) Beta(2)-microglobulin and its deamidated variant, N17D form amyloid fibrils with a range of morphologies in vitro, *J. Mol. Biol. 313*, 559−571.
16. Borysik, A. J., Radford, S. E., and Ashcroft, A. E. (2004) Co-populated conformational ensembles of beta2-microglobulin uncovered quantitatively by electrospray ionization mass spectrometry, *J. Biol. Chem. 279*, 27069−27077.
17. Chiti, F., DeLorenzi, E., Grossi, S., Mangione, P., Giorgetti, S., Caccialanza, G., Dobson, C. M., Merlini, G., Ramponi, G., and Bellotti, V. (2001) A partially structured species of β_2-microglobulin is significantly populated under physiological conditions and involved in fibrillogenesis, *J. Biol. Chem. 276*, 46714−46721.
18. Yamamoto, S., Hasegawa, K., Yamaguchi, I., Tsutsumi, S., Kardos, J., Goto, Y., Gejyo, F., and Naiki, H. (2004) Low concentrations of sodium dodecyl sulfate induce the extension of beta 2-microglobulin-related amyloid fibrils at a neutral pH, *Biochemistry 43*, 11075−11082.
19. Morgan, C. J., Gelfand, M., Atreya, C., and Miranker, A. D. (2001) Kidney dialysis-associated amyloidosis: a molecular role for copper in fiber formation, *J. Mol. Biol. 309*, 339−345.
20. Connors, L. H., Shirahama, T., Skinner, M., Fenves, A., and Cohen, A. S. (1985) *Biochem. Biophys. Res. Commun. 131*, 1063−1068.
21. Esposito, G., Michelutti, R., Verdone, G., Viglino, P., Hernandez, H., Robinson, C. V., Amoresano, A., Dal Piaz, F., Monti, M., Pucci, P., Mangione, P., Stoppini, M., Merlini, G., Ferri, G., and Bellotti, V. (2000) Removal of the N-terminal hexapeptide from human beta2-microglobulin facilitates protein aggregation and fibril formation, *Protein Sci. 9*, 831−845.
22. Drüeke, T. B. (1998) Dialysis-related amyloidosis, *Nephrol., Dial., Transplant. 13*, 58−64.
23. Gorevic, P. D., Munoz, P. C., Casey, T. T., DiRaimondo, C. R., Stone, W. J., Prelli, F. C., Rodrigues, M. M., Poulik, M. D., and Frangione, B. (1986) Polymerization of intact β_2-microglobulin in tissue causes amyloidosis in patients on chronic hemodialysis, *Proc. Natl. Acad. Sci. U.S.A. 83*, 7908−7912.
24. Campistol, J. M., Bernard, D., Papastoitsis, G., Sole, M., Kasirsky, J., and Skinner, M. (1996) Polymerization of normal and intact beta 2-microglobulin as the amyloidogenic protein in dialysis-amyloidosis, *Kidney Int. 50*, 1262−1267.
25. Linke, R. P., Hampl, H., Lobeck, H., Ritz, E., Bommer, J., Waldherr, R., and Eulitz, M. (1989) Lysine-specific cleavage of beta 2-microglobulin in amyloid deposis associated with hemadialysis, *Kidney Int. 36*, 675−681.
26. Bellotti, V., Stoppini, M., Mangione, P., Sunde, M., Robinson, C., Asti, L., Brancaccio, D., and Ferri, G. (1998) Beta-2-microglobulin can be refolded into a native state from ex vivo amyloid fibrils, *Eur. J. Biochem. 258*, 61−67.
27. Stoppini, M. S., Arcidiaco, P., Mangione, P., Giorgetti, S., Brancaccio, D., and Bellotti, V. (2000) Detection of fragments of beta2-microglobulin in amyloid fibrils, *Kidney Int. 57*, 349−350.
28. Monti, M., Principe, S., Giorgetti, S., Mangione, P., Merlini, G., Clark, A., Bellotti, V., Amoresano, A., and Pucci, P. (2002) Topological investigation of amyloid fibrils obtained from beta2-microglobulin, *Protein Sci. 11*, 2362−2369.
29. Miyata, T., Taneda, S., Kawai, R., Ueda, Y., Horiuchi, S., Hara, M., Maeda, K., and Monnier, V. M. (1996) Identification of pentosidine as a native structure for advanced glycation end products in β_2-microglobulin-containing amyloid fibrils in patients with dialysis-related amyloidosis, *Proc. Natl. Acad. Sci. U.S.A. 93*, 2353−2358.
30. Miyata, T., Oda, O., Inagi, R., Iida, Y., Araki, N., Yamada, N., Horiuchi, S., Taniguchi, N., Maeda, K., and Kinoshita, T. (1993) beta 2-Microglobulin modified with advanced glycation end products is a major component of hemodialysis-associated amyloidosis, *J. Clin. Invest. 92*, 1243−1252.
31. Heegaard, N. H. H., Sen, J. W., Kaarsholm, N. C., and Nissen, M. H. (2001) Conformational intermediate of the amyloidogenic protein β_2-microglobulin at neutral pH, *J. Biol. Chem. 276*, 32657−32662.
32. Heegaard, N. H. H., Sen, J. W., and Nissen, M. H. (2000) Congophilicity (Congo red affinity) of different β_2-microglobulin conformations characterized by dye affinity capillary electrophoresis, *J. Chromatogr. A 894*, 319−327.
33. Chiti, F., Mangione, P., Andreola, A., Giorgetti, S., Stefani, M., Dobson, C. M., Bellotti, V., and Taddei, N. (2001) Detection of two partially structured species in the folding process of the amyloidogenic protein beta 2-microglobulin, *J. Mol. Biol. 307*, 379−391.
34. Heegaard, N. H. H., Roepstorff, P., Melberg, S. G., and Nissen, M. H. (2002) Cleaved β_2-microglobulin partially attains a conformation that has amyloidogenic features, *J. Biol. Chem. 277*, 11184−11189.
35. Nissen, M. H., Roepstorff, P., Thim, L., Dunbar, B., and Fothergill, J. E. (1990) Limited proteolysis of beta 2-microglobulin at Lys-58 by complement component C1s, *Eur. J. Biochem. 189*, 423−429.
36. Nissen, M. H., Thim, L., and Christensen, M. (1987) Purification and biochemical characterization of the complete structure of a proteolytically modified beta-2-microglobulin with biological activity, *Eur. J. Biochem. 163*, 21−28.
37. Nissen, M. H., Johansen, B., and Bjerrum, O. J. (1997) A simple method for the preparation and purification of C1 complement cleaved beta 2-microglobulin from human serum, *J. Immunol. Methods 205*, 29−33.
38. Bai, Y., Milne, J. S., Mayne, L., and Englander, S. W. (1993) Primary structure effects on peptide group hydrogen exchange, *Proteins 17*, 75−86.
39. (1989) *The Merck Index*, Merck & Co., Rahway, NJ.
40. Maity, H., Lim, W. K., Rumbley, J. N., and Englander, S. W. (2003) Protein hydrogen exchange mechanism: local fluctuations, *Protein Sci. 12*, 153−160.
41. Okon, M., Bray, P., and Vucelic, D. (1992) ^{1}H NMR assignments and secondary structure of human beta 2-microglobulin in solution, *Biochemistry 31*, 8906−8915.
42. Mori, S., Abeygunawardana, C., Berg, J. M., and van Zijl, P. C. M. (1997) NMR study of rapidly exchanging backbone amide protons in staphylococcal nuclease and the correlation with structural and dynamic properties, *J. Am. Chem. Soc. 119*, 6844−6852.
43. Engen, J. R., Smithgall, T. E., Gmeiner, W. H., and Smith, D. L. (1997) Identification and localization of slow, natural, cooperative unfolding in the hematopoietic cell kinase SH3 domain by amide hydrogen exchange and mass spectrometry, *Biochemistry 36*, 14384−14391.
44. Arrington, C. B., Teesch, L. M., and Robertson, A. D. (1999) Defining protein ensembles with native-state NH exchange: kinetics of interconversion and cooperative units from combined NMR and MS analysis, *J. Mol. Biol. 285*, 1265−1275.
45. LeVine, H. (1993) Thioflavine T interaction with synthetic Alzheimer's disease β-amyloid peptides: Detection of amyloid aggregation in solution, *Protein Sci. 2*, 404−410.
46. Pedersen, J. S., Christensen, G., and Otzen, D. E. (2004) Modulation of S6 fibrillation by unfolding rates and gatekeeper residues, *J. Mol. Biol. 341*, 575−588.
47. Grossman, P. D., Colburn, J. C., and Lauer, H. K. (1989) A semiempirical model for the electrophoretic mobilities of peptides in free-solution capillary electrophoresis, *Anal. Biochem. 179*, 28−33.
48. Zhang, Q., Powers, E. T., Nieva, J., Huff, M. E., Dendle, M. A., Bieschke, J., Glabe, C. G., Eschenmoser, A., Wentworth, P., Jr., Lerner, R. A., and Kelly, J. W. (2004) Metabolite-initiated protein misfolding may trigger Alzheimer's disease, *Proc. Natl. Acad. Sci. U.S.A. 101*, 4752−4757.
49. De Ferrari, G. V., Mallender, W. D., Inestrosa, N. C., and Rosenberry, T. L. (2001) Thioflavin T is a fluorescent probe of the acetylcholinesterase peripheral site that reveals conformational interactions between the peripheral and acylation sites, *J. Biol. Chem. 276*, 23282−23287.
50. Kad, N. M., Myers, S. L., Smith, D. P., Smith, D. A., Radford, S. E., and Thomson, N. H. (2003) Hierarchical assembly of beta2-microglobulin amyloid in vitro revealed by atomic force microscopy, *J. Mol. Biol. 330*, 785−797.
51. Dobson, C. M. (2004) Experimental investigation of protein folding and misfolding, *Methods 34*, 4−14.
52. Canet, D., Last, A. M., Tito, P., Sunde, M., Spencer, A., Archer, D. B., Redfield, C., Robinson, C. V., and Dobson, C. M. (2002)

Local cooperativity in the unfolding of an amyloidogenic variant of human lysozyme, *Nat. Struct. Biol. 9*, 308−315.
53. Dumoulin, M., Last, A. M., Desmyter, A., Decanniere, K., Canet, D., Larsson, G., Spencer, A., Archer, D. B., Sasse, J., Muyldermans, S., Wyns, L., Redfield, C., Matagne, A., Robinson, C. V., and Dobson, C. M. (2003) A camelid antibody fragment inhibits the formation of amyloid fibrils by human lysozyme, *Nature 424*, 783−788.
54. Kelly, J. W. (1996) Alternative conformations of amyloidogenic proteins govern their behavior, *Curr. Opin. Struct. Biol. 6*, 11−17.
55. Dobson, C. M. (1999) Protein misfolding, evolution and disease, *Trends Biochem. Sci. 24*, 329−332.
56. Ozasa, H., Suzuki, T., and Ota, K. (1989) Modification of serum beta-2-microglobulin in chronic hemodialysis patients, *Nephron 53*, 87.
57. Linke, R. P., Hampl, H., Bartel-Schwarze, S., and Eulitz, M. (1987) Beta 2-microglobulin, different fragments and polymers thereof in synovial amyloid in long-term hemodialysis, *Biol. Chem. Hoppe Seyler 368*, 137−144.
58. Jones, S., Manning, J., Kad, N. M., and Radford, S. E. (2003) Amyloid-forming peptides from beta(2)-microglobulin—Insights into the mechanism of fibril formation in vitro, *J. Mol. Biol. 325*, 249−257.
59. Schoels, M., Jahn, B., Hug, F., Deppisch, R., Ritz, E., and Hansch, G. M. (1993) Stimulation of mononuclear cells by contact with cuprophan membranes: further increase of beta 2-microglobulin synthesis by activated late complement components, *Am. J. Kidney Dis. 21*, 394−399.

BI047594T